Supplementary Methods: Experimental

Drosophila strains

Specific strains were *esg-lacZ* (*esg*^{k00606}, Spradling et al., 1999), *Su(H)GBE-GFP:nls* (see below), *N*^{55e11} (Kidd et al., 1983), *l(1)N*^{B} (Lyman and Young, 1993) and *N*^{MCD1} (Ramain et al., 2001).

Clonal analyses were performed on the following genotypes:

- *tub-FRT-lacZ* clones: *y w hs-FLP1.2 / y w; X-15-29 / X-15-33*;
- twin-spot MARCM: *y w hs-FLP1.2 / y w; UAS-GFP:CD8, UAS-CD2-mir, FRT40A / UAS-RFP:CD2, UAS-GFP-mir, FRT40A; tub-Gal4 / +*;
- twin-spot generator: *Df(1) y ac, w hs-FLP1.2 ; Act5C-nGfp-FRT-cRfp / Act5C-nRfp-FRT-cGfp*, using twin-spot generator constructs located at either 38F1 or 82F7.
- MARCM/RFP^{-} twin-spot: *y w hs-FLP1.22; tub-Gal4, UAS-GFP:CD8 / +; tub-Gal80 FRT2A / Histone2A:RFP FRT2A*.

The genotypes for the analysis of ISC:EB ratios in *N* mutant backgrounds was: *N* / +; esg*^{k00606} */ +; Su(H)GBE-GFP:nls / +*, where *N** is either *N*^{55e11}, *l(1)N*^{B}, *N*^{MCD1} or *N*$^{+}$ (Oregon R).

Su(H)GBE-GFP:nls transgene

The *Su(H)GBE* synthetic regulatory fragment (Furriols and Bray, 2001) was amplified by PCR (forward primer: 5'-CACACCTCCCCCTGAACCTGAAACA-3'; reverse primer: 5'-CTCAT*GAATTC*TGTCGCTCCGTAGACGAAGC-3') adding a 3' EcoRI site (italics). From this segment, a 407bp BglII-EcoRI fragment was cloned into the pH-Stinger vector (Barolo et al., 2000).

Long-term lineage tracing

tub-FRT-lacZ flies were dissected at 1 to 28 days after induction and stained for LacZ, F-actin and DNA. Using the F-actin signal, we obtained images of overlapping fields of view covering the whole length of each organ. Each field of view was manually registered and the width, depth and length was recorded, whether it contained clones or not. To calculate the amount of screened tissue, the area of each section was approximated as length * 2 * (width + depth). The region between the pylorus and the stalk of the malpighian tubules was not considered, lest it had some anatomical

specificity. The anterior limit of the posterior section of the midgut was recognized by the characteristic constriction and change in the curvature that delimit the middle midgut. Only organs with intact stalks of the malpighian tubules were used, although some were broken before the constriction.

Wherever clones were found, a z-stack spanning the full thickness of the labelled population was acquired. The clone cell number was counted at least three times, travelling through the z-stack at least once in each direction, until a consistent count was obtained for each clone. For each time point, we collected at least 100 clones from at least 10 different organs, except for day 16 after induction, when the decline in clonal density only allowed the recovery of 55 clones (Supplementary Table S3). Organs from 28 days after induction were not screened for clones, given that they fall outside the time window that we considered ideal for homeostatic maintenance (see below). In agreement with this notion, these guts exhibited frequent pyloric scarring (see below). To allow for quantitative analysis, we made a number of observations to validate the accuracy of the method, discussed next.

Homeostasis and time window – In all our lineage tracing experiments, we induced labelling at least three days after emergence from the puparium, to avoid the period of nutrient-driven post-eclosion growth described by (O'Brien et al., 2011). We considered clone chases up to 23 days of adult life, given that in the midgut, homeostasis breakdown due to aging can occur (at low frequencies) as early as 15 days after eclosion (Biteau et al., 2008). Therefore, we are confident that the majority of our analysis is restricted to the period of adult life when the posterior midgut turnover is homeostatic, although that might not be the case for the last time point of the lineage chase. Notwithstanding our precautions, it was important to obtain indications that the tissue was homeostatic during the long-term chase. We measured the dimensions of the 102 posterior midguts from the experimental cohort that were whole. From our data we estimate the typical posterior midgut to be 1.1 ± 0.2 mm^2 in area and 2.0 ± 0.4 mm in length, with a perimeter of 0.5 ± 0.1 mm (mean ± standard deviation). We observed the average total area at each time point to be fairly uniform throughout the experiment (Supplementary Figure S6B), as expected in homeostasis. Moreover, the cell density was essentially uniform during the first four days of the clonal chase (Supplementary Figure S6C), which, together with the total area measurements, indicates that the tissue

does not experience a significant change in total cell number in the first few days after induction by heat treatment. This is consistent with the tissue being in homeostasis, and not exhibiting a regenerative behaviour. We also recorded the presence of scarring at the pylorus, a kind of lesion that has been associated to regenerative crises (Fox and Spradling, 2009). We observed a substantial increase in the presence of scars and their severity from day 16 after induction (Supplementary Figure S6A), coinciding with the time at which aging-related phenotypes can be detected in the midgut (Biteau et al., 2008). Then we assume that in our lineage tracing experiment, normal homeostasis takes course over a period of less than 16 days following induction.

Specificity of induction – A quantitative analysis of the clone size and density required a tight control over the labelling induction. To evaluate the degree of unspecific labelling, untreated flies from the same cohort were dissected 7, 14 and 21 days of age, stained for LacZ and screened for clones. Spurious induction occurred at very low frequency (Supplementary Figure S2A), which provides high confidence in the specificity of the method.

Response to induction in space and time – We addressed whether clones were specially prone to arise or grow in certain areas. We plotted the number of clones as well as the number of labelled cells against their position along the length of the organ. This reveals a remarkably uniform density of clones and total labelled cells across the tissue at all times (Supplementary Figure S2C-D). Clonal expansion seemed to be delayed for a couple of days following induction (Figure 2B), coinciding with the time of maximal clone density (Figure 2A). This might be due, at least in part, to the labelling strategy. Since most *tub-FRT-lacZ* clones are labelled at mitosis, any synchrony in the timing of cell division time would be reflected in a common lag in clone growth. The accumulation of clones for two days after induction, might be due to perdurance of the FLP protein, resulting in delayed induction of 50% of the cells. This would further add to the observed delay in expansion.

Cell density – We measured clone density as clone number per tissue area unit. To express clone density in cellular terms (Figure 2A), we calculated the cell density in the posterior midgut. We took confocal z-stacks spanning the entire thickness of 16 midgut sections from 11 organs stained for F-actin and DNA. We measured the area and counted the number of cells per section (7540 cells in total), which gave a cell density

value of 4.5 ± 0.8 cells per 1000 μm^2. Considering together our density and organ total area measurements, we estimated that an adult posterior midgut contains ~5000 cells, of which 18% are ISCs (Micchelli and Perrimon, 2006). This corresponds about 900 ISCs per organ, which consistent with published reports (Ohlstein and Spradling, 2006; Choi et al., 2011) and provides additional confidence to our measurements.

Precision of clone identification and size distributions – Clones in the target tissue remain cohesive, which facilitates identification of individual lineages (Ohlstein and Spradling, 2006). However, a number of clones might merge or split. In our inducing conditions, maximal clone density corresponded to one clone per 40 ISCs (Figure 2A). Based on this we estimate that clone merger would affect to about 2% of clones (see Supplementary Methods: Theory). Moreover, we recorded the distances, where below 200μm, between the boundaries of nearest neighbour clones at the time of maximal clone density (day 2). Most clones were separated by more than 200μm (corresponding to more than ten cell diameters), with only less than 4% below 30μm (roughly corresponding to two cell diameters) (Supplementary Figure S2B), which is in good agreement with our estimate. The general compactness of clone shape suggested that clone splitting occurred at low frequencies. However at day 16, when organs have 1.5 clones on average, some clones seemed to be fragments of a larger one – yet these were counted as independent. The *tub-FRT-lacZ* recombination strategy could result in the induction of a post-mitotic clone (Griffin et al., 2009; Harrison and Perrimon, 1993) (see Supplementary Figure S2E). Indeed, we observed weakly labelled polyploid ECs, presumably induced in this manner, as has been reported in the hindgut, midgut, and pupal gut (Jiang and Edgar, 2009; Fox and Spradling, 2009; Mathur et al., 2010; O'Brien et al., 2011; Takashima et al., 2011). Although the frequency of these events is deemed to be minimal, our quantitative analysis required to follow the lineage evolution of an unambiguously defined cell population. Therefore, we limited our attention to clones containing two or more cells, thereby eliminating from consideration non ISC-derived clones.

Twin-spot analyses

Flies were raised and aged at 18ºC to avoid spurious induction during developmental stages, then induced by heat treatment and switched to 25ºC for 2 to 3 days prior to dissection. Twin-spot MARCM seemed the most suitable in promoter homogeneity and

induction specificity. Still, unspecific clonal induction at developmental stages occurred. In all cases, non-induced controls with clones of developmental origin fell in one of these categories: (1) organs with portions of the midgut epithelium covered with large (several tens of cells), abutting twins-pots, or with tracheal twin-spots, and/or with twin-spots at the pylorus and ileum, (2) organs with areas where some small cells, but none of the intervening ECs, were labelled in a single colour, and (3) organs with a solitary epithelial small clone, typically without its twin. In our uninduced controls, we never encountered guts with a regular density of small twinspots (Figure 3D and Supplementary Figure S3A). Therefore we trust these clones are of adult origin.

Statistical analysis

Cell density data from Supplementary Figure 6C were subjected to two-tailed Student's tests. The proportions of ISCs versus EBs found in the different conditions shown in Figure 8A were analyzed by logistic regression. Analyses were performed in MATLAB.

Supplementary Methods: Theory

Clone merger

In the analysis of the lineage tracing study, it is important to ensure that the data is not compromised by clone merger events. If we suppose that the induction protocol leads to the random labelling of cells, an assumption supported by the observed spatial distribution of clones (Supplementary Figure S2C-D), we can make an estimate of the fraction of clones that derive from such events. If we define n as the areal density of labelled clones (measured in Figure 2A as the number of surviving clones per 1000 cells), the mean separation between clones is approximately given by $a \approx 1/\sqrt{n}$ cell diameters. With this definition, it is straightforward to show that the chance of finding the nearest neighbouring clone to be at a separation r is given by

$$P(r) = \frac{2}{a}\left(\frac{r}{a}\right)\exp\left[-\left(\frac{r}{a}\right)^2\right]$$

Then, if we suppose that clones that lie within a distance R cannot be reliably resolved, we would estimate that a fraction,

$$f = \int_0^R P(r)dr = 1 - \exp\left[-\left(\frac{r}{a}\right)^2\right]$$

of clones would be misclassified.

Allowing for the generation of terminally differentiated cell progeny, at a time soon after induction, the critical distance between clones, *R*, would be comparable with a couple of cell diameters while the areal clone density soon after induction has been estimated at $n = 4$ clones per 1000 cells leading to a typical separation of *a* of around 16 cell diameters. This translates to a fraction $f = 0.02$. In other words, soon after induction, we expect some 2% of clones to be misclassified due to merger events.

Through the course of tissue turnover, clones expand while others undergo terminal differentiation and become lost. Although this leads to an expansion of the surviving clones, their typical separation also increases through their attrition. Formally, since the average clone size grows approximately linearly over the timecourse, the effective value of *R* will grow as $\langle n(t) \rangle^{1/2} \propto \sqrt{t}$. At the same time, the density of surviving clones *n* drops approximately as a power law, *1/t*, leading to the separation also increasing as $a \propto \sqrt{t}$. The ratio, *R/a*, therefore stays time-independent leading to the same degree of clone misclassification. Fortunately, the figure of 2% stays well within the error bars of the clone statistics and does, therefore, not adversely effect the conclusions from the analysis.

Modelling scheme

In the main text, we introduced a simple lattice-based modelling scheme to address the detailed behaviour of the clone size distribution prior to the onset of scaling. In this supplementary section, we elaborate on how the properties of the lattice model are inferred from numerical simulation.

To analyse the clonal fate data we considered a 2D array of lineage domains, organized on a regular square lattice. Each lineage domain plays host to four mature terminally differentiated cells (the EC and EE population), an EB type cell, committed to terminal differentiation, and an ISC. For the purpose of the numerical simulation, we will suppose that the lineage specification of the EC and EE type cells from the differentiating EB cell occurs randomly, with probabilities weighted by their respective

population fraction. In this case, it is unnecessary to specify the particular identity of the four terminally differentiated cells. To further define the model, we make two, largely inessential, refinements: First, we will organize the terminally differentiated cells into a hierarchy specified by age with the oldest cell being shed most readily during the course of turnover. Second, to accommodate a refractory period following cell division (which we will find to be fast), we will suppose that the timing between consecutive cell divisions must be in excess of ca. 2/3 of the average cell cycle time, $1/\lambda$. Neither of these refinements impact significantly on the fit to the experimental data.

To address the experimental data, we have the freedom to adjust two model parameters: the average cell division rate, λ (equivalent to the shedding rate of mature terminally differentiated cells from the tissue) and, through r, the frequency of ISC loss/replacement. Algorithmically, the stochastic loss of the oldest mature terminally differentiated cell from tissue leads to a translation of cells along the hierarchy resulting in the specification of the EB type cell (Figure 5B and Supplementary Figure S4). Then, with probability $1-2r$, we suppose that ISC self-renewal in the same domain replenishes the EB type cell. Alternatively, with probability $2r$, we suppose that the EB cell takes on the identity of the partner ISC while the latter is replenished by ISC duplication from a neighbouring domain, chosen at random (Figure 5B and Supplementary Figure S4).

To extract the cellular dynamics of the model, we undertook a numerical simulation of the system with both cell division and fate outcome chosen at random from a Poisson distribution with the appropriate mean, i.e. successive division events and fate outcomes were considered statistically uncorrelated. Once again, any correlation due to synchrony of cell cycle or short-term lineage priming would be rapidly washed out of the experimental data.

From the perspective of genetic labelling, let us consider the possible patterns of clonal evolution. If we begin by labelling one of the differentiated cell types, the resulting single cell clone will persist until it matures and is shed from tissue (Supplementary Figure S4A). In the modelling scheme above, its survival time will belong to a Poisson-like distribution weighted by the "age" of the cell at induction. By contrast, if we label a putative ISC, its clonal evolution may be richer. Following differentiation through division, it may also become shed in the course of turnover (Supplementary Figure S4B). Alternatively, through cell division with fate asymmetry, its self-renewal can lead

to the progressive expansion of the clone to occupy its lineage domain (Supplementary Figure S4A). Finally, if the ISC in the neighbouring domain is lost, the clone may expand to occupy more than one lineage domain (Supplementary Figure S4B). Taken together, ISC-derived clones are predicted to follow a pattern of neutral drift in which the continual extinction of clones due to ISC loss is compensated by the progressive expansion of neighbouring clones. The process leads to a progressive coarsening of the clonal composition, illustrated by the simulation shown in Supplementary Figure S7. (Note that the process of ISC loss and replacement can lead to the fragmentation of clones as unlabeled cells can "invade" labelled tissue leading to the isolation of labelled fragments.)

To draw comparison of the model with the data, we examined the distribution of total clone size, focusing on clones with a size of two cells or more. The latter form a defined population, which can only be derived from cells within the progenitor cell pool. Referring to the measured clone size distribution (Figure 2C, E), the development of a pronounced minimum in the distribution of small clones from 3 days post-induction onwards suggests that the majority of cell divisions leading to asymmetric fate outcome: Recall that for $r = 0$, we recover the model of invariant asymmetry. In this case, ISC-derived clones expand to occupy their clonal unit. As a result, the peak in the probability distribution is predicted to shift progressively towards the size of the clonal unit (set at six) leaving behind a minimum for smaller clone sizes. As r is increased, this feature is gradually diminished as symmetrical ISC division and loss lead to divergent fates.

As discussed in the main text, taking a lattice size of 500x500 lineage domains, a comparison of the model to the clone size data shows an excellent fit over the first 8 days following induction, if we set the ISC division rate to $\lambda = 2.5$/day and $r = 0.1$ (Figure 2E). Here we have included a time off-set of 1.2 days following induction which accounts for the accumulation of labelled cells following heat-shock, and the nature of the induction protocol which leads to induction following division (Supplementary Figure S2E). The same parameters provide an equally good fit to the survival curve (Figure 2A) and the internal clone composition (Figure 4B-C).

Legends to supplementary figures

Supplementary Figure S1. Apical view of the *Drosophila* midgut epithelium

View of the *Drosophila* midgut epithelium from Figure 1B, showing expression of Arm and Pros (red), *esg-lacZ* (blue), and *Su(H)GBE-GFP:nls* (green), and DNA (gray) in separate panels.

Supplementary Figure S2. The *tub-FRT-lacZ* labelling method and its application to the posterior midgut

(**A**) Untreated flies displayed labelled clones at very low frequencies throughout the time window of the long-term lineage tracing experiment (black line). For comparison, the clonal density values of the parallel lineage tracing experiment are also plotted (red line). The numbers are in clones per organ. In the case of the lineage tracing density values, they were obtained for this figure by converting the clone density (number per unit area) into whole organ equivalents, applying the measurement obtained for average total area). Thinner lines depict values ± the standard deviation of the organ size measurement.
(**B**) Cumulative distribution of nearest-neighbour inter-clone distances at day 2 after induction of the long-term lineage tracing.
(**C, D**) By recording both the position and size of the surviving clones throughout the chase period following induction, we could measure the spatial distribution of label density along the length of the posterior midgut. This is plotted here as the cumulative number of clones (A) or total labelled cells (B) per gut section against the length of screened tissue, at 1, 2, 3, 4, 5, 8 and 16 days post-induction. Here we show data from all of the organs screened at each timepoint arranged consecutively (see Supplementary Table S3 for organ number). The uniformity of the spatial distribution is consistent with an unbiased process of induction and a spatially uniform turnover of the tissue.
(**E**) Recombination strategy of the *tub-FRT-lacZ* method and possible outcomes (see also Harrison and Perrimon, 1993). Recombination occurs between the *αTub84B* promoter and the *βGal:nls* coding sequence, at a syntenic genomic location, and it is mediated by the FRT/FLP system (Golic and Lindquist, 1989). In principle the transcription unit can be reconstituted at either G0, G1 (upper branch) or G2 (lower branch), only the latter guaranteeing the stem cell-origin of the clone (note that only one stem cell daughter will be labelled). Mitotic recombination is considered the most frequent event (see main text).

Supplementary Figure S3. Multi-cellular twin clones with alternative methods.

(**A-A'**) Twin spots using the twin-spot MARCM generator method (Yu et al., 2009), showing sparse induction (see also Figure 3D). The dashed square corresponds to the area shown in Figure 3F.
(**B-B'**) Multicellular twin spot using the twin-spot generator method (Griffin et al., 2009).
(**C-D**) Multicellular twin-spot tracing by labelling with the loss of Histone2A:RFP versus the gain of GFP. As a result, green and unlabelled multi-cellular sister clones can be recognized against a red background (C-C''). The method is based on MARCM (Lee and Luo, 1999): by exchanging Gal80 and Histone2A:RFP, one sibling inherits double dose of Histone2A:RFP and de-represses UAS-GFP, while the other loses nuclear RFP signal (D). In D it is assumed the presence of a ubiquitous Gal4 driver, not depicted in the schematic for simplicity.

Supplementary Figure S4. Clonal pathways in the model of tissue homeostasis

(**A**) In a model of invariant asymmetry, the loss of a mature terminally differentiated cell alongside the differentiation of an EB always promote the division of an ISC in the same domain, which self-renews and replenishes the EB lost through terminal differentiation. This series of concatenated replacements is depicted in frame (a), upper left domain. As a result, stem cell clones are immortal, whereas non-stem cell clones will be transient and lost over the course of turnover. In (a), a labelled ISC (red) divides to replace lost cells in its domain, while a labelled EB (magenta) undergoes terminal differentiation to substitute a lost mature cell. Over time (b, c), the red ISC clone grows while the magenta EB turns into a fully differentiated EC and dies. Finally, the red ISC clone reaches the steady state, occupying the lineage domain, whereas the transient EB clone disappears (d).
(**B**) In a model of population asymmetry, the loss of a mature terminally differentiated cell alongside the differentiation of an EB can promote the division of an ISC in the same domain. Alternatively, if both esg^+ cells in a lineage domain have undergone cell cycle exit, the loss of a terminally differentiated cell alongside the differentiation of an EB cell must be compensated by the duplication of an ISC in a neighbouring domain. The first two frames (a, b) show the development of these two pathways for two previously labelled ISCs. In the first case, the clone (red) expands within one lineage

domain. In the second (magenta), cells in two neighbouring domains become labelled. Following the differentiation of a labelled ISC and its replacement through the division of an unlabelled cell in the neighbouring domain, the next frame (c) shows the appearance of a two-cell clone (red) in which both cells have exited cell cycle. By contrast, the second clone (magenta) has undergone expansion. Over time, the first clone will become lost while the second clone may go on to expand further (d). To model the system, we suppose differentiation of an EB leads to cell division of the partner ISC in the same domain with a probability 1-2*r* while, with probability 2*r*, the loss is compensated by symmetrical duplication of the neighbouring ISC. (To gain further mechanistic insight into these processes, we refer to Figure 5 and the discussion.)

(**C**) The correlation of ISC loss and replacement following the division of proximate cells provides a natural mechanism to realize the model of population asymmetric self-renewal defined in (B) and the main text (see Figure 5B).

Supplementary Figure S5. N^{MCD1} is Delta-dependent

N^{MCD1}/+ phenotype is rescued by simultaneous heterozygosity in *Dl*. (**A-C**) Dorsal toraces of wild-type (A), N^{MCD1}/+ (B) and N^{MCD1}/+;; Dl^{rev10}/+ (C) flies. Note that the balding pattern in (B), especially in the area between the dorsocentral and supraalar bristles (arrowhead) and between the prescutal sutures (asterisk) is ameliorated in (C). (**D**) Microchaeate number (mean ± standard deviation) in wild-type, N^{MCD1}/+ and N^{MCD1}/+;; Dl^{rev10}/+ flies, showing the extent of the rescue of N^{MCD1} by Dl^{rev10}. (**E-G**) Wings of wild-type (E), N^{MCD1}/+ (F) and N^{MCD1}/+;; Dl^{rev10}/+ (G) flies. Note in F that along with distal nicks (arrowhead), the wings have tears (asterisk). These tears were present in all flies and were not caused by the mounting or the aging of the flies. They probably originate during the emergence from the puparium, since the N^{MCD1}/+ wings appear to be very brittle. The N^{MCD1}/+;; Dl^{rev10}/+ double heterozygous wings in G are essentially wild-type.

Supplementary Figure S6. Organ size and of pyloric scarring in the lineage tracing cohort

(**A**) Presence of scars in the pylorus in the long-term experimental cohort. Pyloric scarring is absent or negligible until 16 days after induction (corresponding to ~3 weeks

after emergence). Photographs show examples of none, medium and strong scarring, as labelled.
(**B**) Evolution of total midgut area in the long-term tracing experiment (average ± standard deviation in black and gray). Sample sizes are given above the *x* axis. The global average is marked in discontinuous gray.
(**C**) Evolution of cell density in cells per field of view (FOV, equivalent to ~0.1mm^2) over the first four days of the long-term tracing experiment. Whiskers in the box plots show the data of the upper and lower quartiles within 1.5 times the interquartile range.

Supplementary Figure S7. Coarsening of the lineage composition in the simulations

(**A-B**) Illustrative images of the lineage composition of the 2D model. In the early stage of turnover (A), most domains are populated by its original lineage. As homeostasis proceeds, every loss and replacement event leads to a progressive and irreversible impoverishment of the clonal composition of the tissue, which translates into the observed coarsening of the lineages (B).

Supplementary Movie S1.

Animated z-stack of the *tub-FRT-lacZ* clone with a single Dl$^+$ cell, corresponding to Figure 3A. The left panel shows the lineage marker lacZ (red), Dl (green) and DNA (blue). The right panel shows Dl in greyscale. Dl$^+$ cells are surrounded by a circle.

Supplementary Movie S2.

Animated z-stack of the *tub-FRT-lacZ* clone containing no Dl$^+$ cells, which corresponds to Figure 3B. The left panel shows the lineage marker lacZ (red), Dl (green) and DNA (blue). The right panel shows Dl in greyscale. Dl$^+$ cells are surrounded by a circle.

Supplementary Movie S3.

Animated z-stack of the *tub-FRT-lacZ* clone with three Dl$^+$ cells, corresponding to Figure 3C. The left panel shows the lineage marker lacZ (red), Dl (green) and DNA (blue). The right panel shows Dl in greyscale. Dl$^+$ cells are surrounded by a circle.

Supplementary Movie S4.

Animated z-stack of the twin-spot MARCM clone shown in Figure 3F. The left panel shows the lineage markers CD8:GFP (green), CD2:RFP (red) and DNA (blue). The central panel shows a single lineage marker, CD2:RFP (red) and DNA (cyan). The right panel shows a single lineage marker, CD8:GFP (green), and DNA (magenta).

Supplementary tables

Supplementary Table S1. Size and composition of the esg$^+$ cell nests

number of clusters	number of EBs per cluster: 0	1	2	3	4	5
0		226	39	5	1	0
1	346	244	63	7	0	0
2	28	8	1	0	2	0
3	8	0	0	0	0	1
4	0	0	0	0	0	0
5	0	0	0	0	0	0
6	0	0	0	0	0	0
7	1	0	0	0	0	0

(number of ISCs per cluster)

Total number of clusters:	980
Singletons	572
Pairs	311
Trios	84
Quartets	9
EB-only clusters:	271
Multiple ISC clusters:	45

Total number of cells:	1502
EBs	737
ISCs	765

Supplementary Table S2. Short-term lineage composition

(See SupplementaryTableS2.xlsx file)

Supplementary Table S3. Scale of the long-term clonal analysis

Time point	Number of clones	Number of organs
1	115	10
2	228	13
3	195	16
4	147	17
5	101	24
8	100	36
16	55	35
Total:	941	151

Supplementary references

Barolo, S., Carver, L.A. and Posakony, J.W. (2000) GFP and beta-galactosidase transformation vectors for promoter/enhancer analysis in Drosophila. *Biotechniques*, **29**, 726, 728, 730, 732.

Furriols, M. and Bray, S. (2001) A model Notch response element detects Suppressor of Hairless-dependent molecular switch. *Curr Biol*, **11**, 60-64.

Golic, K.G. and Lindquist, S. (1989) The FLP recombinase of yeast catalyzes site-specific recombination in the Drosophila genome. *Cell*, 59, 499-509.

Griffin, R., Sustar, A., Bonvin, M., Binari, R., del Valle Rodriguez, A., Hohl, A.M., Bateman, J.R., Villalta, C., Heffern, E., Grunwald, D., Bakal, C., Desplan, C., Schubiger, G., Wu, C.T. and Perrimon, N. (2009) The twin spot generator for differential Drosophila lineage analysis. *Nat Methods*, 6, 600-602.

Harrison, D.A. and Perrimon, N. (1993) Simple and efficient generation of marked clones in Drosophila. *Curr Biol*, 3, 424-433.

Kidd, S., Lockett, T.J. and Young, M.W. (1983) The Notch locus of Drosophila melanogaster. *Cell*, **34**, 421-433.

Lee, T. and Luo, L. (1999) Mosaic analysis with a repressible cell marker for studies of gene function in neuronal morphogenesis. *Neuron*, 22, 451-461.

Lyman, D. and Young, M.W. (1993) Further evidence for function of the Drosophila Notch protein as a transmembrane receptor. *Proc Natl Acad Sci U S A*, **90**, 10395-10399.

Mathur, D., Bost, A., Driver, I. and Ohlstein, B. (2010) A transient niche regulates the specification of Drosophila intestinal stem cells. *Science*, **327**, 210-213.

O'Brien, L.E., Soliman, S.S., Li, X. and Bilder, D. (2011) Altered modes of stem cell division drive adaptive intestinal growth. *Cell*, **147**, 603-614.

Ramain, P., Khechumian, K., Seugnet, L., Arbogast, N., Ackermann, C. and Heitzler, P. (2001) Novel Notch alleles reveal a Deltex-dependent pathway repressing neural fate. *Curr Biol*, **11**, 1729-1738.

Takashima, S., Younossi-Hartenstein, A., Ortiz, P.A. and Hartenstein, V. (2011) A novel tissue in an established model system: the Drosophila pupal midgut. *Dev Genes Evol*, **221**, 69-81.

Yu, H.H., Chen, C.H., Shi, L., Huang, Y. and Lee, T. (2009) Twin-spot MARCM to reveal the developmental origin and identity of neurons. *Nat Neurosci*, **12**, 947-953.

Supplementary Figure S1

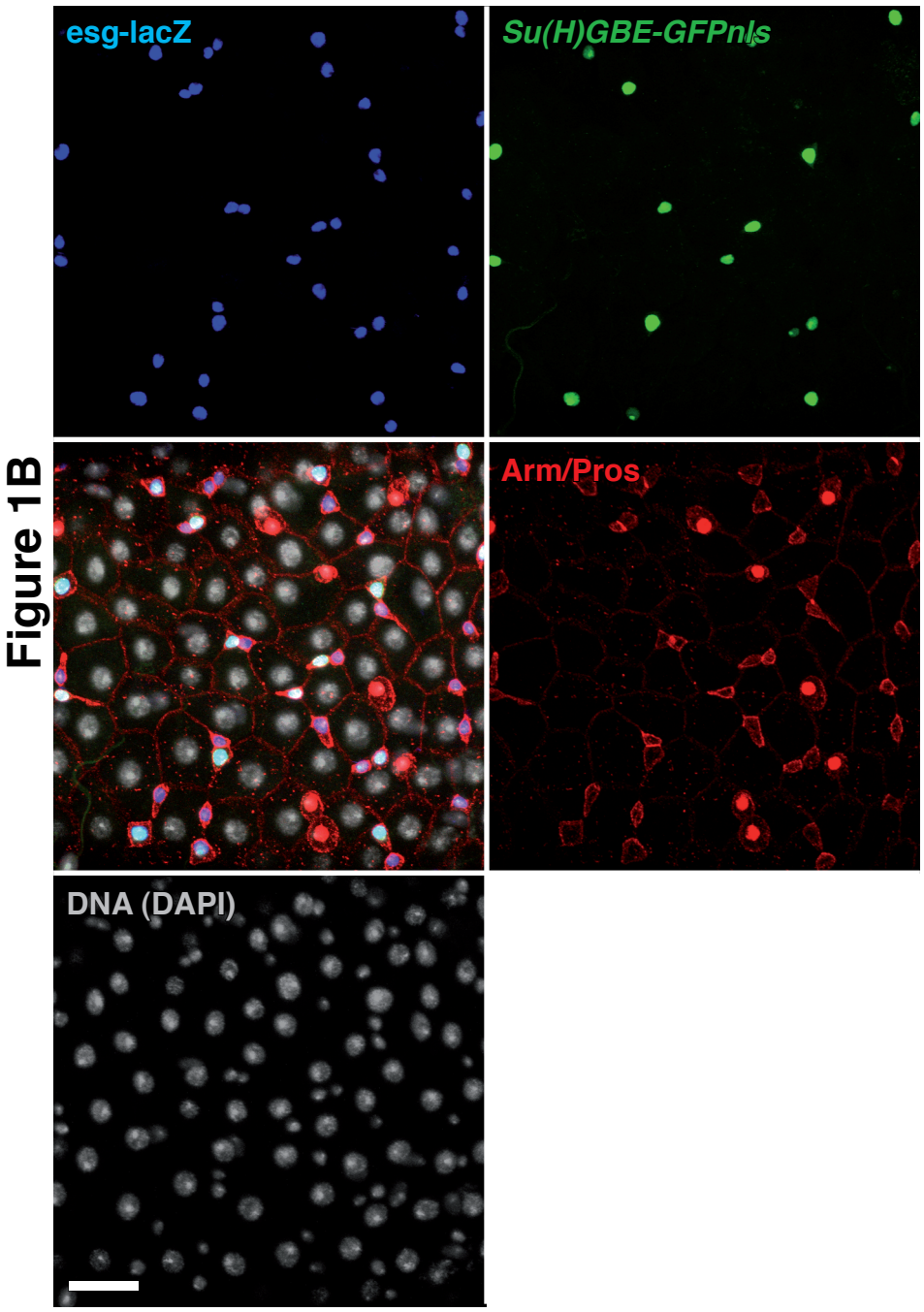

Figure 1B

Supplementary Figure S2

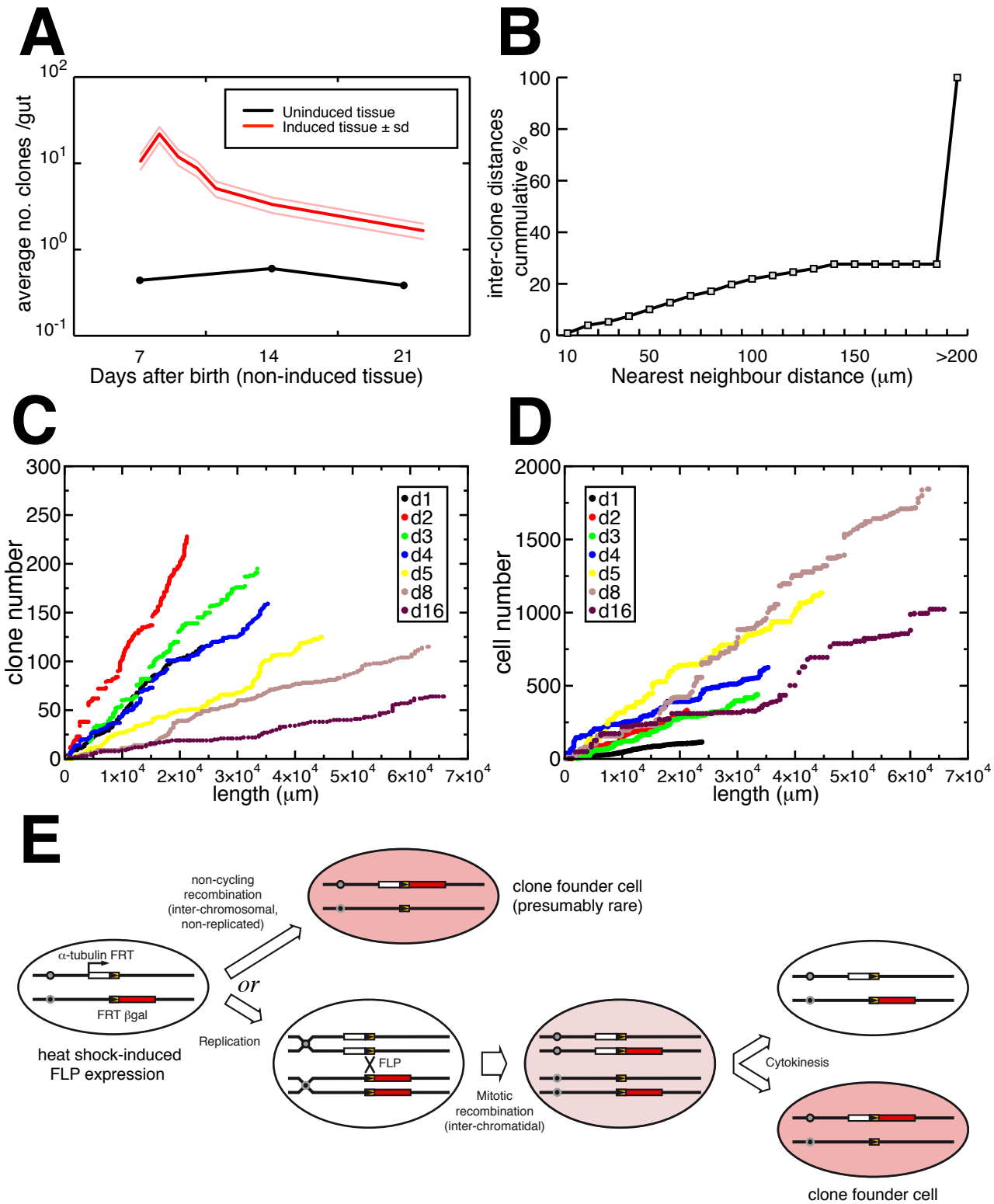

Supplementary Figure S3

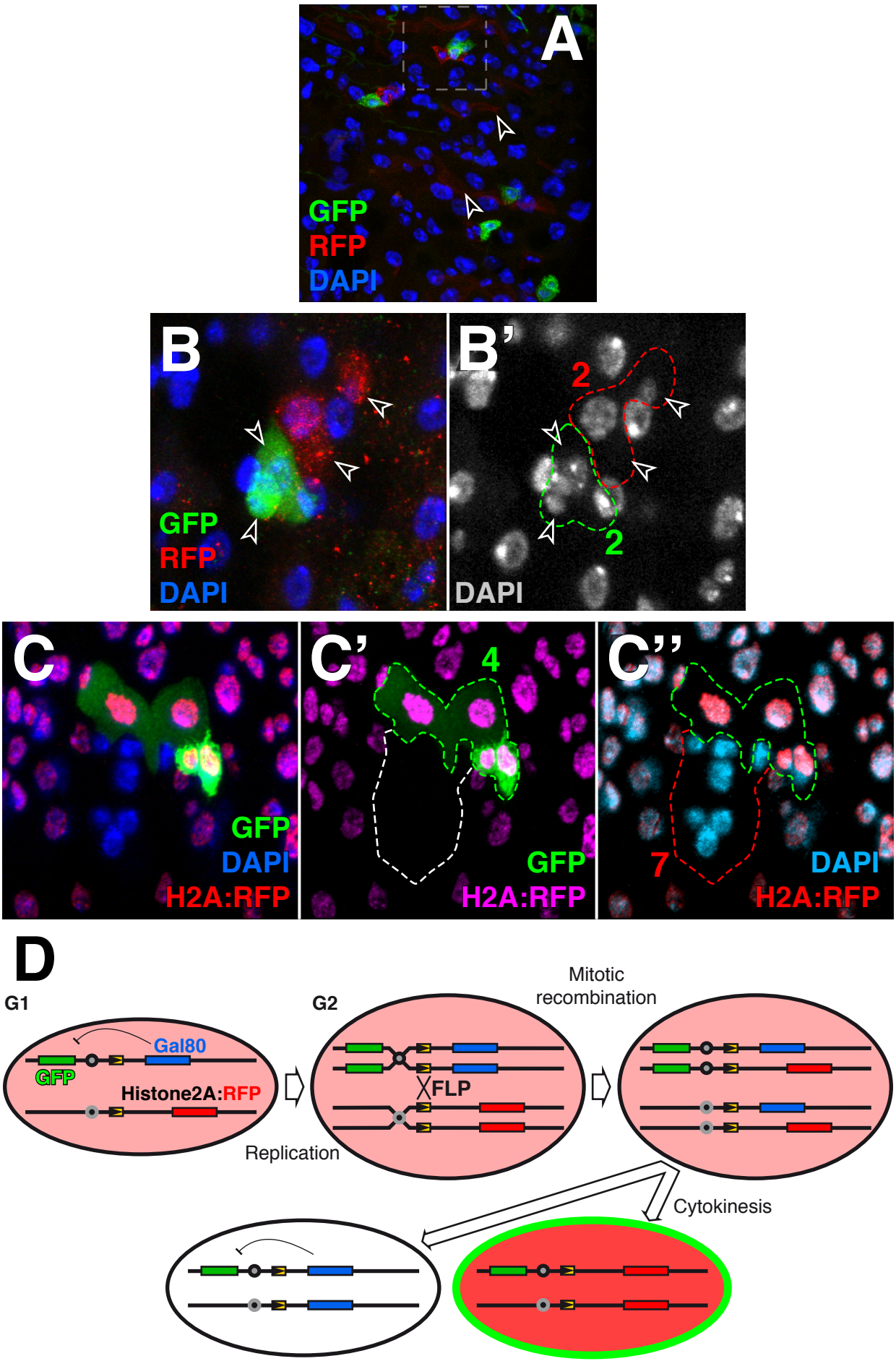

Supplementary Figure S4

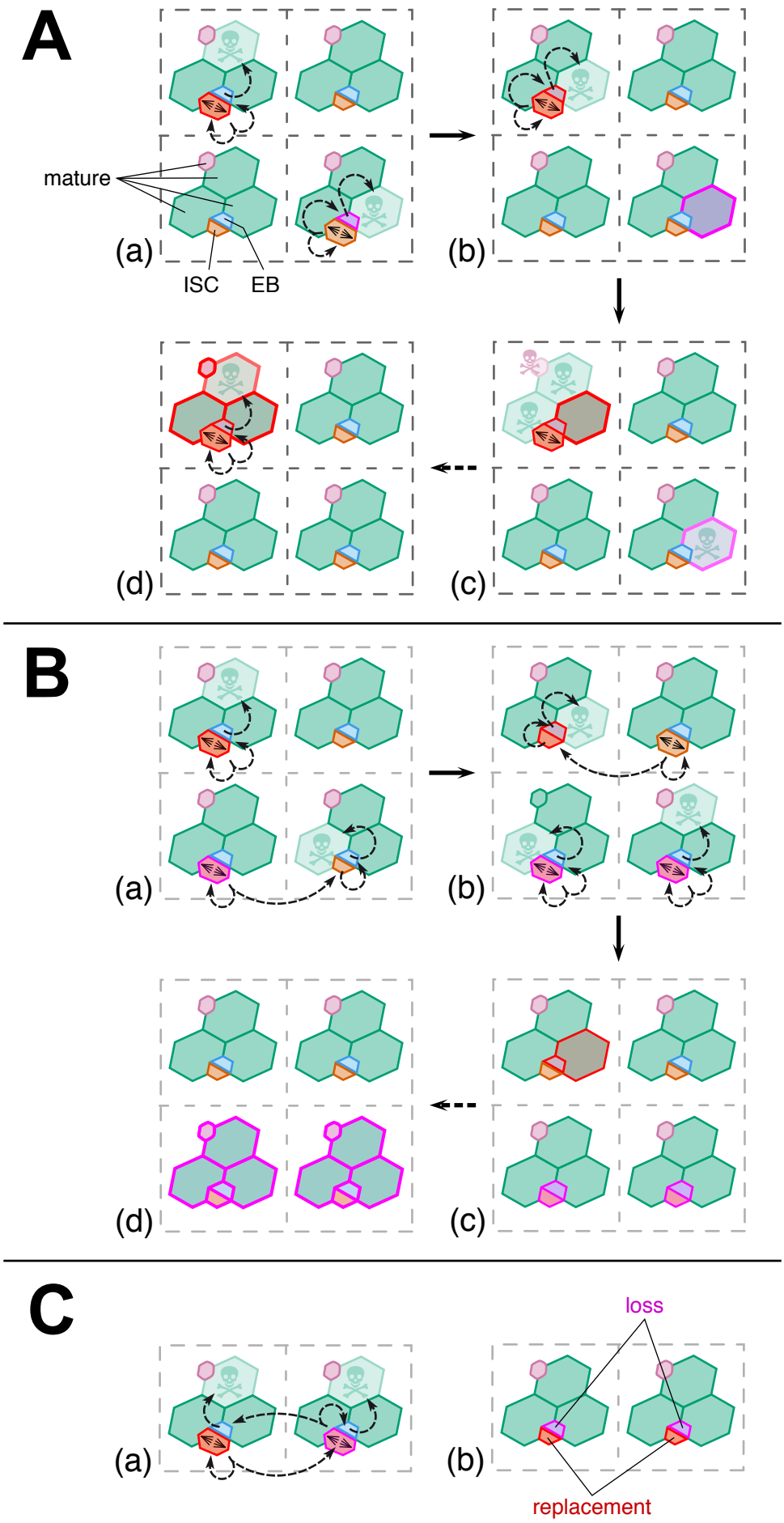

Supplementary Figure S5

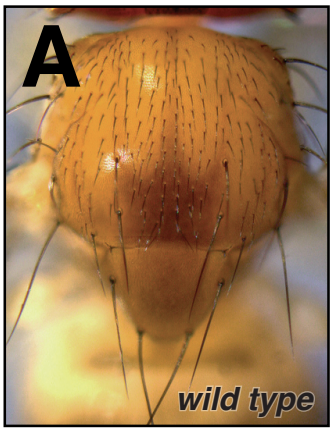

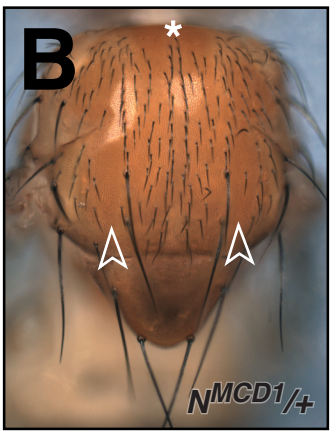

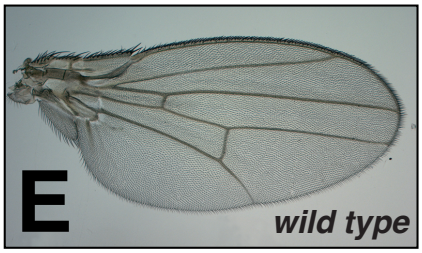

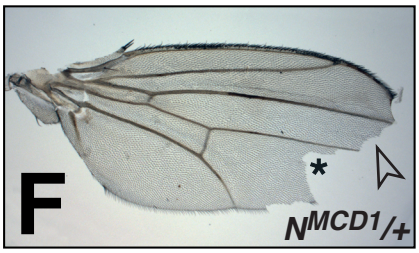

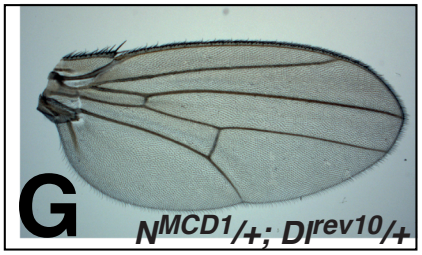

D

Number of microchaetae per notum

wild type	*260 ±10*
$N^{MCD1}/+$	*186 ± 9*
$N^{MCD1}/+$;; $Dl^{rev10}/+$	*224 ± 4*

Supplementary Figure S6

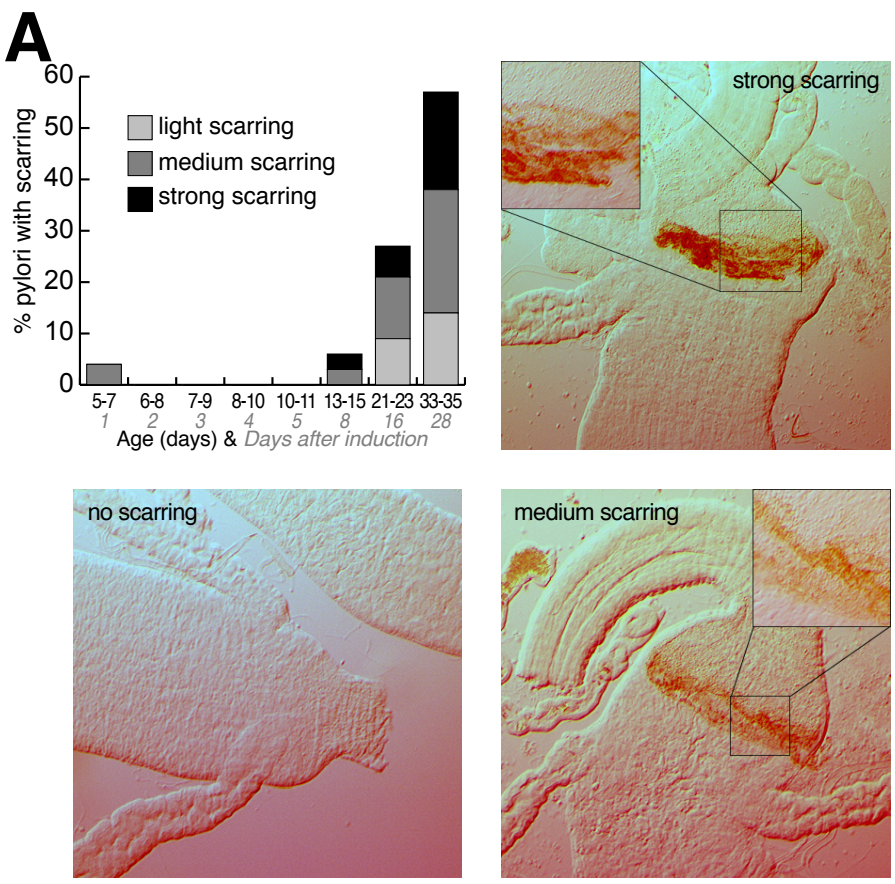

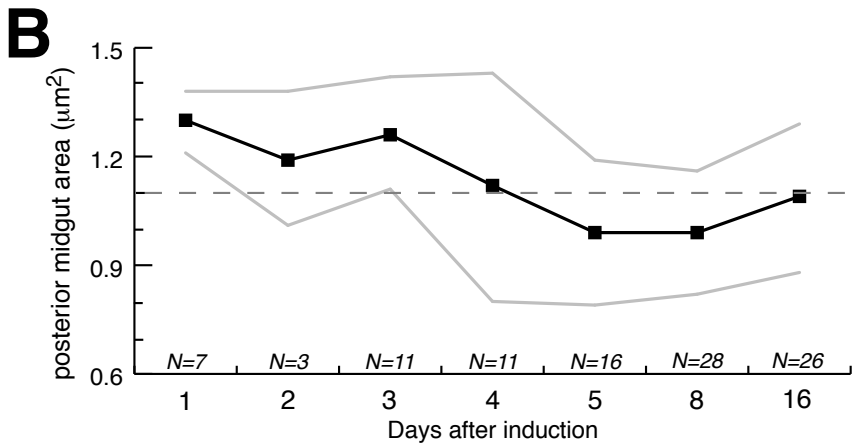

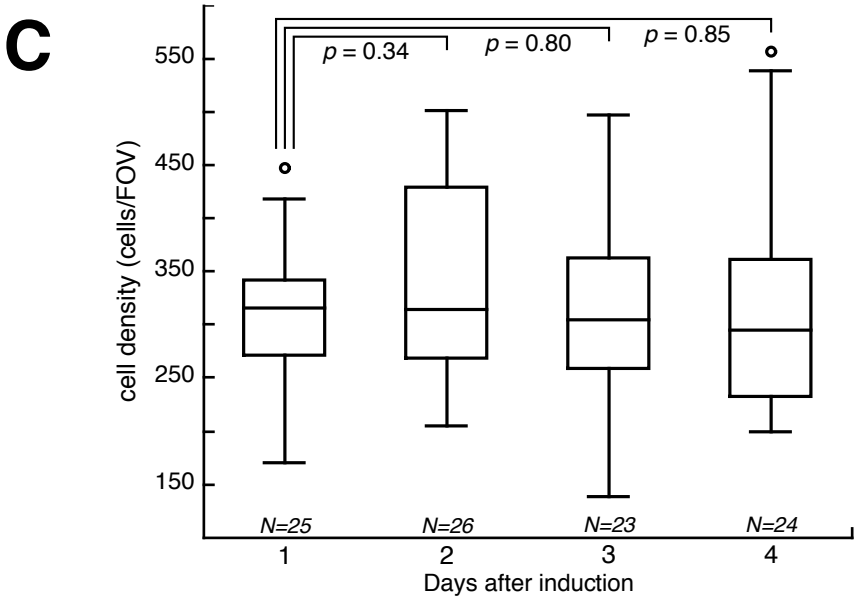

Supplementary Figure S7